High Photovoltage in Perovskite Solar Cells: New Physical Insights from the Ultrafast Transient Absorption Spectroscopy

M. Ibrahim Dar[a]*, Marius Franckevičius[b], Neha Arora[a], Kipras Redeckas[c], Mikas Vengris[c], Vidmantas Gulbinas[b], Shaik Mohammed Zakeeruddin[a], Michael Grätzel[a]*

[a] *Laboratory of Photonics and Interfaces, Department of Chemistry and Chemical Engineering, Swiss Federal Institute of Technology Lausanne, Lausanne CH-1015, Switzerland.*

[b] *Center for Physical Sciences and Technology, Saulėtekio Ave. 3, LT-10257 Vilnius, Lithuania*

[c] *Department of Quantum Electronics, Faculty of Physics, Vilnius University, Saulėtekio Ave. 10, LT-10223 Vilnius, Lithuania*

*Correspondence authors: (M.I.D.) E-mail: ibrahim.dar@epfl.ch, (M.G.) E-mail: michael.graetzel@epfl.ch

Abstract

To understand the cause of the high open circuit photovoltage (V_{OC}) achieved by todays' state of the art perovskite solar cells (PSCs), we examine formamidinium lead bromide $CH(NH_2)_2PbBr_3$) films by ultrafast transient absorption spectroscopy (TAS). The devices based on the $CH(NH_2)_2PbBr_3$ films yield V_{OC} as high as 1.5 V ascertaining their high quality. TAS establish that the presence of charge extraction layers has very little influences on the nature of a negative band at 535 nm corresponding to the bleaching of the absorption band edge and two positive bands in the $CH(NH_2)_2PbBr_3$ films. Therefore, we contend that the V_{OC} in PSC is predominantly determined by the quasi Fermi level splitting within the perovskite layer.

Keywords: perovskite solar cells, photovoltage, charge carrier dynamics, transient absorption spectroscopy

1. Introduction

Perovskite solar cells (PSC) have shown a remarkable growth in terms of high photovoltaic performance. Within a decade from their inception, the certified power conversion efficiency (PCE) of PSC has already exceeded 22% [1]. Owing to the extraordinary optoelectronic properties of perovskite absorbers, such a remarkable evolution in the PCE has been realized [2].

For the first time Kojima et al. reported a PCE of 3.8% when mesoporous TiO_2 was sensitized with $CH_3NH_3PbI_3$, subsequently, Park and coworkers improved the PCE to >5% [3,4]. In both reports, the liquid dye-sensitized solar cell (DSC) architecture was retained. Ageing tests revealed that these solar cells are unstable, and such issues were found to be associated with the dissolution of perovskite material in the liquid electrolyte. Intuitively, the solid-state DSC architecture was an alternative option, which was adopted and PCE exceeding 9% was reported by Park and co-workers, and Snaith and co-workers [5,6].

Although record efficiency yielding PSCs still involve charge extraction layers which were actually used for solid-state DSC, there are certain sharp differences [7,8]. For example, unlike dye molecules, perovskite absorbers are ambipolar in nature [6] and the V_{OC} has been found to show minimal dependence on the band positions in the charge extraction layers [9]. Using mesoporous TiO_2 and spiro-OMeTAD, respectively, as electron and hole extraction layers, which were initially introduced by Graetzel and co-workers in the solid-state DSC [10], high V_{OC} could be extracted from the bromide PSC. Using mesoporous Al_2O_3 as an insulating scaffold, Cahen and coworker, reported a V_{OC} of 1.3 V for $CH_3NH_3PbBr_3$ based devices [11]. Arora et al. demonstrated the deposition of high quality of $CH(NH_2)_2PbBr_3$ films and their application in PSC for achieving a V_{OC} of 1.42 V [12]. After improving the growth of $CH_3NH_3PbBr_3$ layer by inducing the heterogeneous nucleation using HBr, Im and co-worker achieved a V_{OC} of 1.5 V

[13]. Recently, Arora et al. achieved a photovoltage of 1.53 V for $CH(NH_2)_2PbBr_3$ solar cells by modifying the interface between mesoporous TiO_2 and $CH(NH_2)_2PbBr_3$ layer using lithium treatment [14].

Recently, remarkable efficiencies have brought PSCs to the forefront of the photovoltaic application; however, their fundamental studies are still evolving, For example, the origin of the outstanding photovoltage (V_{OC}) exhibited by PSC still needs to be explored as this is a key photovoltaic metrics that has led to an exceptional evolution in their performance. To gain deeper physical insights into the high V_{OC}, we selected the relatively less explored $CH(NH_2)_2PbBr_3$ perovskite material which is distinguished by a high stability as a case study system [15]. We unraveled the influence of charge extraction layers on the excited state charge carrier dynamics by ultrafast transient absorption spectroscopy (TAS), and correlated the results with the outstanding V_{OC} displayed by the $CH(NH_2)_2PbBr_3$ solar cells.

2. Materials and methods

All materials were purchased from Sigma-Aldrich and were used as received unless stated otherwise.

2.1. Preparation of TiO_2 photoanode

Fluorine-doped tin oxide (FTO)-glass substrates (NSG 10, Nippon sheet glass, Japan) were cleaned by ultrasonication in Hellmanex (2%, deionized water), rinsed thoroughly with de-ionized water and ethanol, and then treated in oxygen plasma for 15 min. Using a commercial titanium diisopropoxide bis(acetylacetonate) solution (75% in 2-propanol, Sigma-Aldrich) diluted in anhydrous ethanol (1:9, volume ratio) as precursor and oxygen as a carrier gas, a

compact layer of TiO_2 of ca 30 nm was subsequently deposited via spray pyrolysis at 450 °C. A mesoporous TiO_2 layer was then deposited by spin coating a diluted paste (1:3.5 wt. ratio) (Dyesol 30NRD: ethanol) (5000 rpm, acceleration 2000 rpm for 30 s) atop of the compact TiO_2 layer. This was followed by a series of sintering steps (325 °C for 5 min with 15 min ramp time, 375 °C for 5 min with 5 min ramp time, 450 °C for 30 min with 5 min ramp time) in dry air. For lithium treatment of mesoporous TiO_2 photoanode, 200 µL of bis(trifluoromethylsulfonyl)imide lithium salt solution in acetonitrile (20 mg/mL, freshly prepared in argon atmosphere) was spin coated (3000 rpm, acceleration 2000 rpm for 20 s) after a loading time of 10 s, and the substrates were subjected to a second sintering step at 450 °C for 30 min. 250 nm-thick Al_2O_3 mesoporous layer composed of 30 nm Al_2O_3 nanoparticles was deposited on non-conducting glass substrate by spin coating diluted paste (1:3.5 wt. ratio) (5000 rpm, acceleration 2000 rpm for 30 s). The mesoporous Al_2O_3 films were obtained after sintering the substrates at 450 °C for 30 min with 10 min ramp time.

2.2. Device fabrication

$CH(NH_2)_2PbBr_3$ films were deposited using two-step sequential deposition method [15]. 1.2 M $PbBr_2$ (TCI 99%) precursor solution was prepared in *N*,*N*-dimethylformamide (DMF, Acros Organics) and dimethylsulphoxide (DMSO, Acros Organics) by constant stirring at 60 °C for 30 minutes. $PbBr_2$ (DMF+DMSO in 1:1 volume ratio) solution was spin-coated onto the mesoporous TiO_2 films at 3000 rpm for 30 s. After heating at 80 °C for 15 min, the $PbBr_2$ films were dipped into $CH(NH_2)_2$ solution (Dyesol, 50 mM) in isopropanol for 5 min at 60 °C, rinsed with 2-propanol for 5 s and dried at 80 °C for 30 min. 72.3 mg spiro-OMeTAD (2,2',7,7'-tetrakis(*N*,*N*-di-*p*-methoxyphenylamine)-9,9-spirobifluorene) was dissolved in 1 mL of chlorobenzene, to which 28.8 µL 4-tert-butylpyridine, 17.5 µL of a stock solution of

520 mg mL^{-1} bis(trifluoromethylsulfonyl)imide lithium salt in acetonitrile, and 29 μL of a stock solution of 300 mg mL^{-1} tris(2-(1H-pyrazol-1-yl)-4-tert-butylpyridine)cobalt(III) bis(trifluoromethylsulphonyl)imide in acetonitrile were added. The device fabrication was carried out under controlled atmospheric conditions with humidity <1%. Finally, device fabrication was completed by thermally evaporating ~70 nm of gold layer as a back contact.

2.3.Morphological characterization

Field-emission scanning electron microscope (FESEM, Merlin) was employed to analyze the morphology of the $CH(NH_2)_2PbBr_3$ devices. An electron beam accelerated to 3 kV was used with an in-lens detector.

2.4. Device characterization

The current-voltage (J-V) characteristics of the $CH(NH_2)_2PbBr_3$ devices were recorded with a digital source meter (Keithley model 2400, USA). A 450 W xenon lamp (Oriel, USA) was used as the light source for photovoltaic measurements. The spectral output of the lamp was filtered using a Schott K113 Tempax sunlight filter (Präzisions Glas & Optik GmbH, Germany) to reduce the mismatch between the simulated and actual solar spectrum to less than 2%. The photo-active area of 0.16 cm^2 was defined using a dark-coloured metal mask.

2.5. Spectroscopic characterization

UV-Vis extinction spectra were recorded with a Jasco V-670 spectrophotometer in the range of 300-1000 nm. The experimental setup used for the femtosecond-resolution absorption pump-probe experiments was introduced in Ref [16]. In brief, the measurement system is based on the Ti:Sa femtosecond system COHERENT LIBRA (3.5 W, 50 fs, 987 Hz). The pump radiation at

500 nm was generated with a travelling-wave optical parametric amplifier (OPA) TOPAS-800 pumped with ca. 20% of the fundamental Ti:Sa system output. White light supercontinuum generated in a mechanically translated 3 mm thick CaF_2 plate was used as the broadband probe light. Polarizations of pump and probe beams were set at the "magic" angle (54.7°). The probe beam was dispersed using a Czerny–Turner type imaging spectrograph (NEWPORT ORIEL 127I) and the entire NUV-to-NIR probe spectrum was digitized and read out with the 512 pixel linear photodiode array (HAMAMATSU 8380-512Q). In order to avoid permanent damage, the sample films were slowly (ca. 0.1 mm/s) translated transversely to the beam propagation direction using two perpendicularly-aligned motorized linear stages.

3. Results and discussion

Fig. 1a shows cross sectional scanning electron microscopy (SEM) micrograph of the complete $CH(NH_2)_2PbBr_3$ solar cell, which clearly brings out the thickness of various layers comprising the device. Typically, the device fabrication involves the deposition of ~400 nm thick $CH(NH_2)_2PbBr_3$ onto ~250 nm thick mesoporous TiO_2 supported on a transparent conducting glass containing pre-deposited compact (~30 nm) TiO_2 layer. Subsequently, the device is completed by depositing ~180 nm thick spiro-OMeTAD layer and by thermally evaporating a ~70 nm thick gold layer as a back contact. The photovoltaic performance of the resulting devices was investigated by recording the current-voltage (JV) characteristics under standard full sun illumination **(Fig. 1b)**. The $CH(NH_2)_2PbBr_3$ device showed a short circuit current density (J_{SC}) of 6.86 mA/cm^2, an open-circuit voltage (V_{OC}) of 1.5 V, and a fill factor (FF) of 70 % resulting in an overall PCE of 7.3%. In addition, the device exhibited a negligible hysteresis (**Fig. S1**). Such photovoltaic parameters are in close agreement with the literature [14].

Given the conduction band position of TiO_2 and the highest occupied molecular orbital (HOMO) of spiro-OMeTAD, respectively, as 4.0 and 5.1 eV, a V_{OC} of ~1.1 V is expected [17]. However, we obtain a V_{OC} of 1.5 V for our $CH(NH_2)_2PbBr_3$ devices that cannot be rationalized using this simplistic approach and therefore demands critical evaluation.

In principle, nature of charge carrier recombination dynamics dictate the efficiency of the light harnessing and light emitting devices [18].. Therefore, to understand the excited state dynamics of charge carriers, $CH(NH_2)_2PbBr_3$ films were examined by means of ultrafast transient absorption spectroscopy (TAS). Transient absorption (TA) spectra and decay kinetics of $CH(NH_2)_2PbBr_3$ perovskite films deposited onto insulating mesoporous Al_2O_3 excited at 500 nm are shown in **Fig. 2**. The steady state absorption spectrum is also plotted for clarity. Transient absorption spectra show a negative band at 535 nm corresponding to the bleaching of the absorption band edge and two positive bands on either side of the negative band (**Fig. 2a)**. The TA spectral features of $CH(NH_2)_2PbBr_3$ perovskite are quite similar to those observed in other related perovskites, thus could be explained using existing conceptions [19,20]. The bleaching band is attributed to the valence band (VB) depopulation [21] and the positive long-lived induced absorption band in a 490-520 nm region arises due to refractive index change [20] The bleaching band shows an initial fast red shift, which could be attributed to the exciton-exciton interaction [22]. The photo-induced bleach is directly related to the carrier density, thus by tracking absorption recovery, we can characterize carrier recombination and extraction processes.

Immediately after photoexcitation, hot charge carriers are generated resulting in the appearance of a short lived positive TA signal slightly above the band gap at about 550 nm. Subsequently, carrier cooling takes place on a hundreds of femtoseconds (fs) time scale as

reflected by TA decay kinetics (**Fig. 2b**). The thermalization lifetime in the $CH(NH_2)_2PbBr_3$ perovskite could be attributed to the hot-phonon bottleneck effect [20,23].

To gain more information about the charge carrier recombination process in $CH(NH_2)_2PbBr_3$ perovskite films, we additionally measured the TA kinetics at various excitation intensities (5-100 $\mu J \cdot cm^{-2}$) (**Fig 3**). Assuming that bimolecular recombination merely governs the carrier dynamics on a several nanosecond (ns) time scale, we can express the carrier decay kinetics by the rate equation $dn/dt = -\gamma(t)n^2$. For disordered systems, the time-dependent recombination may be approximated by the rate law $\gamma(t) = \gamma_0 t^{-\alpha}$, [24] and solution of the rate equation gives the carrier concentration kinetics: $1/n - 1/n_0 = \gamma_0 t^{1-\alpha} / (1-\alpha)$ Assumming that the carrier concentration is proportional to ΔA, we plot $1/\Delta A - 1/\Delta A_0 = f(t)$ in double logarithmic coordinates. In this representation, concentration kinetics at different excitation intensities coincides and closely follows a linear dependence validating the proposed approach. Slope of the curves gives $\alpha \approx 0.35$, which shows that the carrier recombination rate at all excitation intensities decreases with time as $t^{-0.35}$. The time-dependence of the recombination rate apparently originates from the polycrystalline perovskite structure, where grain boundaries create obstacles for the carrier motion reducing carrier recombination rate at longer times when carriers migrate between crystallites. Excitation intensity-independent kinetics also indicates that carrier trapping and trap saturation suggested in the literature do not take place in our samples in the investigated time domain [25]. Some deviation from the linear dependence at long times observed at very high excitation intensities indicates that carrier decay rate in these conditions is slightly faster than determined by the $t^{-0.35}$. Such a dependence cannot be caused by the trap saturation, which is expected to give opposite deviation. This reflects a complex recombination kinetics in the polycrystalline fractal-like structure.

To study the effect of electron and hole transporting materials on the carrier dynamics, we measured TA kinetics in $CH(NH_2)_2PbBr_3$ films interfaced with the mesoporous TiO_2 layer or spiro-MeOTAD or both layers (**Fig 4**). Negligible enhancement of the carrier decay rate on a several nanosecond time scale was observed for $CH(NH_2)_2PbBr_3$ perovskites. It shows that the carrier injection from photoexcited perovskite into the charge extraction layers is slow in comparison with the investigated time domain. This also agrees with the results of previous studies showing that the charge extraction from other perovskites occur on tens to hundreds of nanoseconds time scale [26].

Fig. 5 schematically illustrates various processes, including charge injection, charge carrier recombination and relaxation occurring within the PSC after photoexcitation. Vertical dotted arrows represent excitation of electrons from the VB of perovskite into its CB, red solid curves describe injection of electrons and holes, respectively, into the CB of TiO_2 and the HOMO of spiro-OMeTAD. Relatively thick inverted yellow colored arrow represents a radiative recombination occurring within the perovskite absorber layer. In other words, the radiative recombination of charge carriers majorly occur within the $CH(NH_2)_2PbBr_3$ layer immediately after photo-excitation, which evidently contends that the band positions in the charge extraction layers play negligible role in determining V_{OC} in PSC. Furthermore, as the position of CB in TiO_2 and HOMO of spiro-OMeTAD is 4.0 and 5.1 eV, respectively, a V_{OC} of ~1.5 V will be difficult to explain using the conventional approach.

4. Conclusion

While using mesoporous TiO_2 and spiro-OMeTAD as charge extraction layers, the devices based on $CH(NH_2)_2PbBr_3$ films revealed outstanding V_{OC} of 1.5 V, ascertaining their high quality. To

understand the causation of such a remarkable V_{OC}, the $CH(NH_2)_2PbBr_3$ films deposited onto mesoporous Al_2O_3 were examined by ultrafast transient absorption spectroscopy as the charge carrier dynamics occurring within the absorber layer critically influence the V_{OC}. Transient absorption spectra show a negative band at 535 nm corresponding to the bleaching of the absorption band edge. Due to the generation of hot carriers, a short lived positive TA signal at ~550 nm appears, which decays on a hundreds of fs time scale. Astoundingly, the impact of extraction layers, i.e., TiO_2 and spiro-OMeTAD, on the nature of charge carrier dynamics occurring within the $CH(NH_2)_2PbBr_3$ films was found to be insignificant. From the results obtained through TAS, we establish that the quasi Fermi level splitting within the $CH(NH_2)_2PbBr_3$ layer predominantly determine the V_{OC} or the presence of charge extraction layers minimally influence the V_{OC} in the PSCs.

Acknowledgement

M. I. D., S. M. Z. and M. G. thank the King Abdulaziz City for Science and Technology (KACST) and Swiss National Science Foundation (SNSF) for financial support. M.F. and V.G. acknowledge funding from the Research Council of Lithuania via grant No. LAT-07/2016. N. A. gratefully acknowledges financial support from Dyesol.

References

[1] National Renewable Energy Laboratory Best Research-Cell Efficiencies; www.nrel.gov/ncpv/images/efficiency_chart.jpg.

[2] M.I. Dar, G. Jacopin, S. Meloni, A. Mattoni, N. Arora, A. Boziki, S.M. Zakeeruddin, U. Rothlisberger, M. Grätzel, Sci. Adv. 2 (2016), e1601156.

[3] A. Kojima, K. Teshima, Y. Shirai, T. Miyasaka, J. Am. Chem. Soc. 131 (2009) 6050.

[4] J.-H. Im, C.-R. Lee, J.-W. Lee, S.-W. Park, N.-G. Park, Nanoscale 3 (2011) 4088.

[5] H.-S. Kim, C.-R. Lee, J.-H. Im, K.-B. Lee, T. Moehl, A. Marchioro, S.-J. Moon, R. Humphry-Baker, J.-H. Yum, J.E. Moser, M. Grätzel, N.-G. Park, Sci. Rep. 2 (2012) 591.

[6] M.M. Lee, J. Teuscher, T. Miyasaka, T.N. Murakami, H.J. Snaith, Science 338 (2012) 643.

[7] N.J. Jeon, J.H. Noh, W.S. Yang, Y.C. Kim, S. Ryu, J. Seo, S.I. Seok, Nature 517 (2015) 476.

[8] D. Bi, C. Yi, J. Luo, J.-D. Décoppet, F. Zhang, Shaik M. Zakeeruddin, X. Li, A. Hagfeldt, M. Grätzel, Nature Energy 1 (2016) 16142.

[9] R.A. Belisle, P. Jain, R. Prasanna, T. Leijtens, M.D. McGehee, ACS Energy Letters 1 (2016) 556.

[10] U. Bach, D. Lupo, P. Comte, J.E. Moser, F. Weissortel, J. Salbeck, H. Spreitzer, M. Gratzel, Nature 395 (1998) 583.

[11] E. Edri, S. Kirmayer, M. Kulbak, G. Hodes, D. Cahen, J. Phys. Chem. Lett. 5 (2014) 429.

[12] N. Arora, M.I. Dar, M. Hezam, W. Tress, G. Jacopin, T. Moehl, P. Gao, A.S. Aldwayyan, B. Deveaud, M. Grätzel, M.K. Nazeeruddin, Adv. Funct. Mater. 26 (2016) 2846.

[13] J.H. Heo, D.H. Song, S.H. Im, Adv. Mater. 26 (2014) 8179.

[14] N. Arora, M.I. Dar, M. Abdi-Jalebi, F. Giordano, N. Pellet, G. Jacopin, R.H. Friend, S.M. Zakeeruddin, M. Grätzel, Nano Letters 16 (2016) 7155.

[15] J. Burschka, N. Pellet, S.J. Moon, R. Humphry-Baker, P. Gao, Md.K. Nazeeruddin, M.

Grätzel, Nature, 499 (2013), 316-319.

[15] A.A. Zhumekenov, M.I. Saidaminov, M.A. Haque, E. Alarousu, S.P. Sarmah, B. Murali, I. Dursun, X.-H. Miao, A.L. Abdelhady, T. Wu, O.F. Mohammed, O.M. Bakr, ACS Energy Letters 1 (2016) 32.

[16] K. Redeckas, V. Voiciuk, R. Steponavičiūtė, V. Martynaitis, A. Šačkus, M. Vengris, , J. Phys. Chem. A 118 (2014) 5642.

[17] W.H. Nguyen, C.D. Bailie, E.L. Unger, M.D. McGehee, J. Am. Chem. Soc. 136 (2014) 10996.

[18] K. Tvingstedt, O. Malinkiewicz, A. Baumann, C. Deibel, H.J. Snaith, V. Dyakonov, H.J. Bolink, Sci. Rep. 4 (2014) 6071.

[19] J.C. Brauer, Y.H. Lee, M.K. Nazeeruddin, N. Banerji, J. Phys. Chem. Lett. 6 (2015) 3675.

[20] M.B. Price, J. Butkus, T.C. Jellicoe, A. Sadhanala, A. Briane, J.E. Halpert, K. Broch, J.M. Hodgkiss, R.H. Friend, F. Deschler, Nat. Commun. 6 (2015) 8420.

[21] J.S. Manser, P.V. Kamat, Nat Photon 8 (2014) 737.

[22] P. Piatkowski, B. Cohen, F. Javier Ramos, M. Di Nunzio, M.K. Nazeeruddin, M. Gratzel, S. Ahmad, A. Douhal, Phys. Chem. Chem. Phys. 17 (2015) 14674.

[23] Y. Yang, D.P. Ostrowski, R.M. France, K. Zhu, J. van de Lagemaat, J.M. Luther, M.C. Beard, Nat Photon 10 (2016) 53.

[24] T. Tiedje, A. Rose, Solid State Comm. 37 (1981) 49.

[25] Y. Yamada, T. Yamada, A. Shimazaki, A. Wakamiya, Yanemitsu J. Phys. Chem. Lett. 7 (2016) 1972.

[26] Q. Shen, Y. Ogomi, J. Chang, S. Tsukamoto, K. Kukihara, T. Oshima, N. Osada, K. Yoshino, K. Katayama, T. Toyoda, S. Hayase, Phys. Chem. Chem. Phys 16 (2014) 19984.

Figure Captions

Fig. 1. Morphological analysis and photovoltaic study of $CH(NH_2)_2PbBr_3$ solar cell. (a) Cross-sectional SEM image of a complete device and (b) Current-voltage curve recorded form $CH(NH_2)_2PbBr_3$ device under standard illumination at 0.05 V/s scan rate.

Fig. 2. (a) Transient absorption spectra and (b) decay kinetics of $CH(NH_2)_2PbBr_3$ perovskite deposited onto insulating mesoporous Al_2O_3 layer, following excitation at 500nm with an average pump energy density of 5.5 $\mu J \cdot cm^{-2}$. The dotted gray line in (a) shows steady state absorption spectrum.

Fig. 3. Intensity dependent transient absorption decay kinetics of $CH(NH_2)_2PbBr_3$ perovskite at 535 nm shown as the time dependence of $1/\Delta A - 1/\Delta A_0$.

Fig. 4. Transient absorption spectra of $CH(NH_2)_2PbBr_3$ perovskite films deposited onto (a) mesoporous TiO_2 layer, (b) interfaced between spiro-OMeTAD and TiO_2, and (c) spiro-OMeTAD and Al_2O_3, following excitation at 500nm with an average pump energy density of 5.5 $\mu J \cdot cm^{-2}$. The dotted gray lines in all figures show steady state absorption spectra of corresponding samples.

Fig. 5. Scheme showing photoexcitation, charge carrier recombination and relaxation processes occurring within the perovskite solar cell. Inverted yellow color displays that the charge carrier recombination occurs predominantly within the perovskite absorber layer, and dark dotted circle represents trap-assisted recombination.

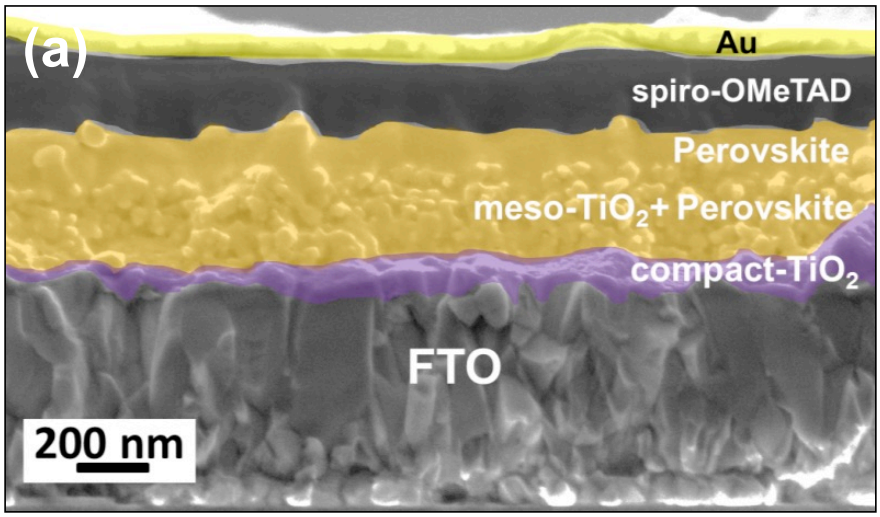
(a)
Au
spiro-OMeTAD
Perovskite
meso-TiO2+ Perovskite
compact-TiO2
FTO
200 nm

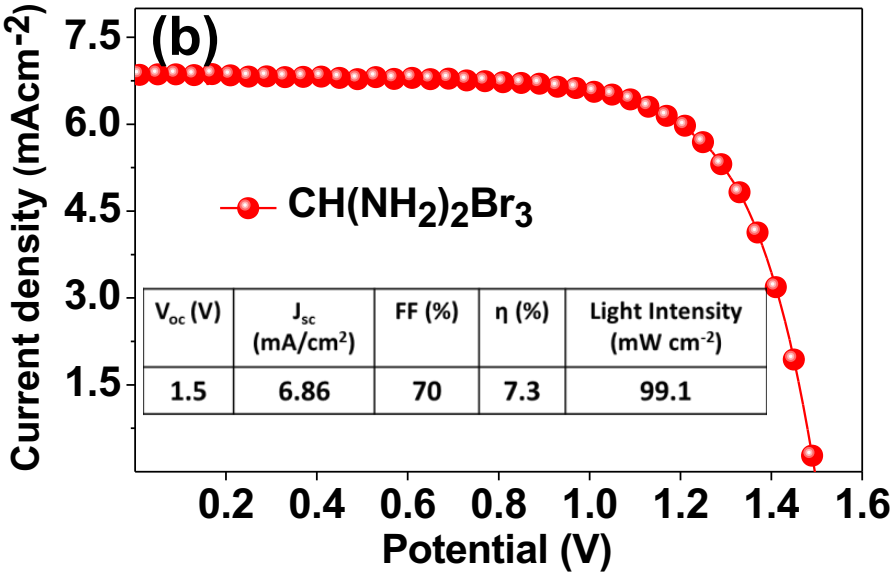
(b)
Current density (mAcm-2)
7.5
6.0
4.5
3.0
1.5
CH(NH2)2Br3
Voc (V) | Jsc (mA/cm2) | FF (%) | η (%) | Light Intensity (mW cm-2)
1.5 | 6.86 | 70 | 7.3 | 99.1
0.2 0.4 0.6 0.8 1.0 1.2 1.4 1.6
Potential (V)

Fig. 1. Morphological analysis and photovoltaic study of $CH(NH_2)_2PbBr_3$ solar cell. (a) Cross-sectional SEM image of a complete device and (b) Current-voltage curve recorded form $CH(NH_2)_2PbBr_3$ device under standard illumination at 0.05 V/s scan rate. (Ibrahim please add a graph with the IPCE data plus their integration over the AM1.5 solar emission to this Figure !. Also hysteresis should be discussed.) (Neha included hysteresis data (Fig. S1), but we don't have IPCE data, which will be provided during revision).

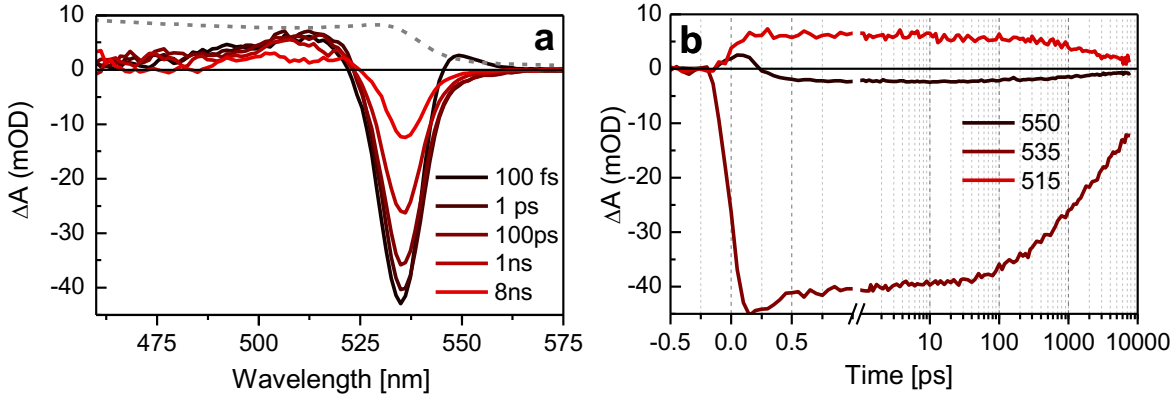

Fig. 2. (a) Transient absorption spectra and (b) decay kinetics of $CH(NH_2)_2PbBr_3$ perovskite deposited onto insulating mesoporous Al_2O_3 layer, following excitation at 500nm with an average pulse energy density of 5.5 $\mu J \cdot cm^{-2}$. The dotted gray line in (a) shows steady state absorption spectrum.

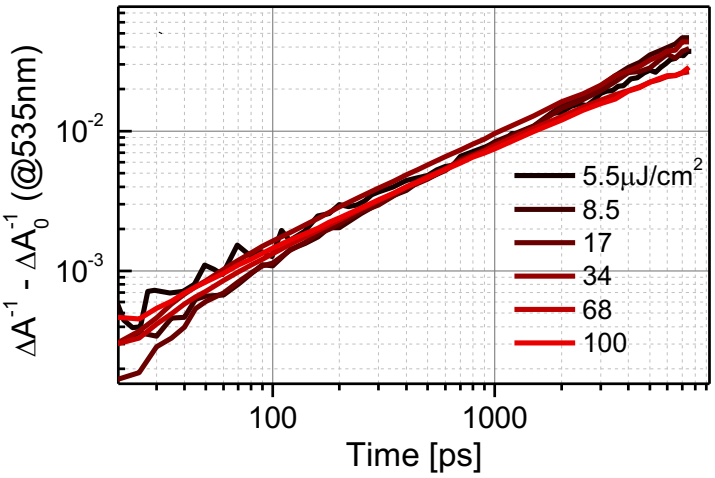

Fig. 3. Intensity dependent transient absorption decay kinetics of $CH(NH_2)_2PbBr_3$ perovskite at 535 nm shown as the time dependence of $1/\Delta A$-$1/\Delta A_0$.

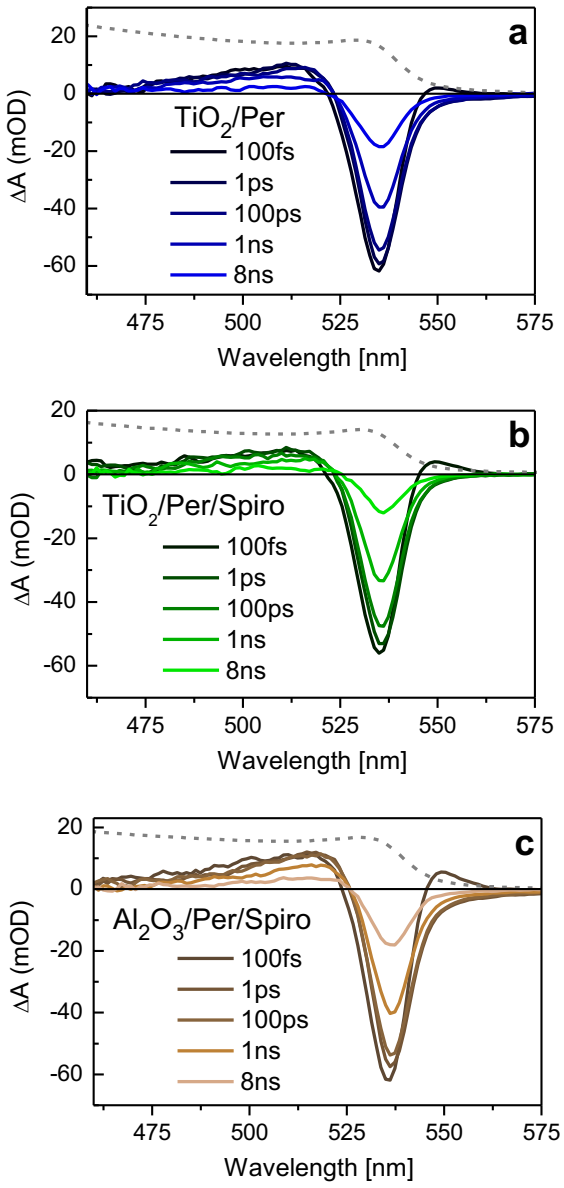

Fig. 4. Transient absorption spectra of $CH(NH_2)_2PbBr_3$ perovskite films deposited onto (a) mesoporous TiO_2 layer, (b) interfaced between spiro-OMeTAD and TiO_2, and (c) spiro-OMeTAD and Al_2O_3, following excitation at 500nm with an average pump energy density of 5.5

$\mu J \cdot cm^{-2}$. The dotted gray lines in all figures shows steady state absorption spectra of corresponding samples.

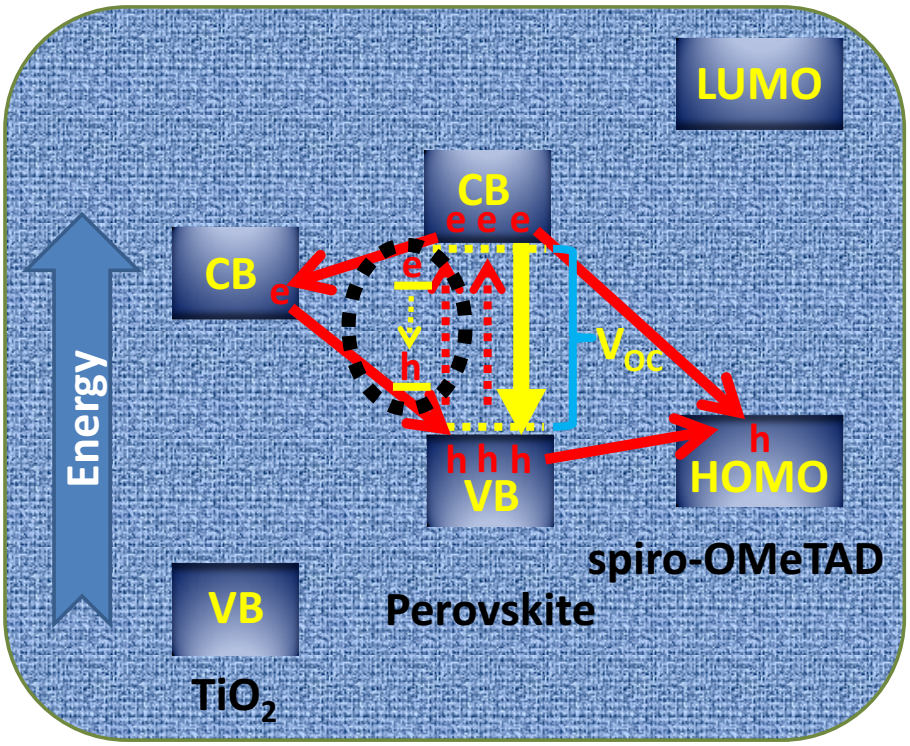

Fig. 5. Scheme showing photo-excitation, charge carrier injection, recombination and relaxation processes occurring within the perovskite solar cell. Inverted yellow color shows that the charge carrier recombination occurs predominantly within the perovskite absorber layer and dotted circle (dark color) represents trap-assisted recombination.

Graphical Abstract

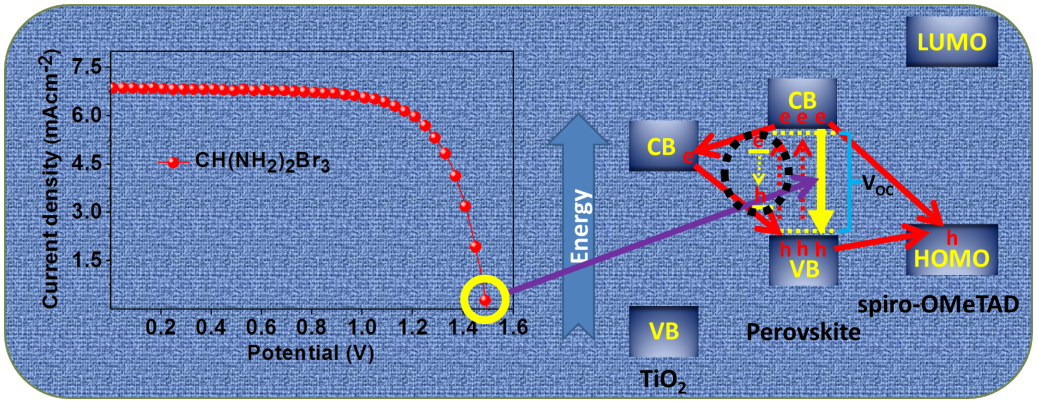

Highlights

- The critical understanding and the origin of V_{OC} as high as 1.5 V displayed by $CH(NH_2)_2PbBr_3$ solar cells is presented.
- In case of $CH(NH_2)_2PbBr_3$, a negative band at ~535 nm corresponding to the bleaching of the absorption band edge, and two positive absorption bands were revealed by transient absorption spectroscopy.
- We found that the presence of charge extraction layers exhibit insignificant effect on the excited state charge carrier dynamics in $CH(NH_2)_2PbBr_3$ films.
- We contend that the quasi Fermi level splitting within the absorber layer predominantly determine the V_{OC} in PSC.

Supporting information

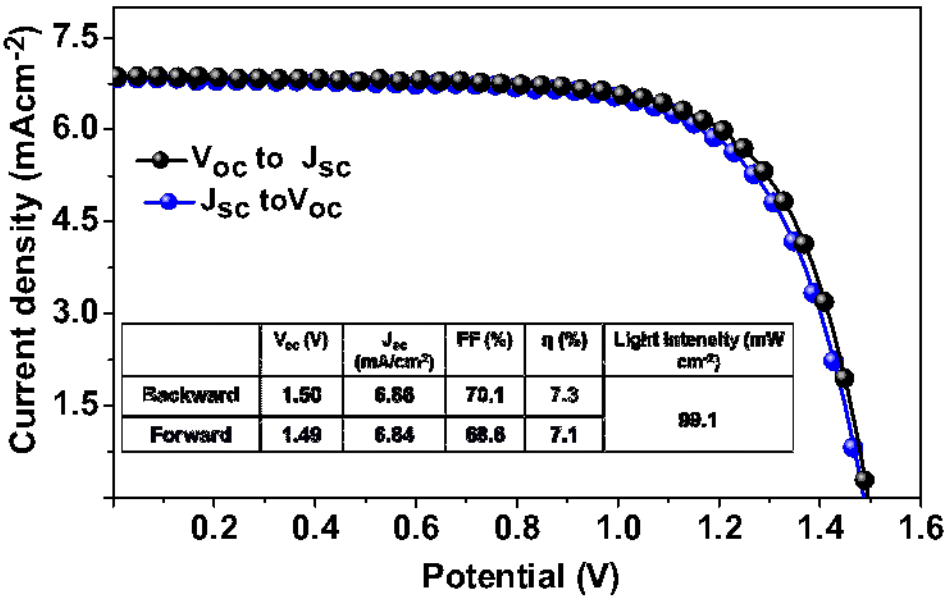

	V_{oc} (V)	J_{sc} (mA/cm^2)	FF (%)	η (%)	Light intensity (mW cm^{-2})
Backward	1.50	6.66	70.1	7.3	99.1
Forward	1.49	6.64	68.6	7.1	

Fig. S1. Current-voltage hysteresis curve recorded form $CH(NH_2)_2PbBr_3$ device under standard illumination at 0.05 V/s scan rate.

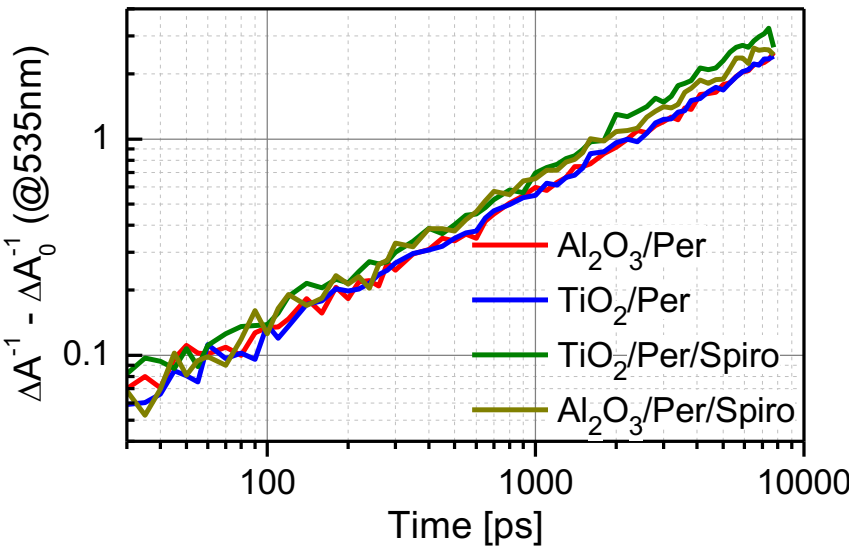

Fig. S2. Intensity dependent transient absorption decay kinetics of $CH(NH_2)_2PbBr_3$ perovskites films interfaced with charge extracting and insulating layers at 535 nm shown as the time dependence of $1/\Delta A$-$1/\Delta A_0$.